Electronic structure of free-standing InP and InAs nanowires

B. Lassen[a)]
Department of Physics, University of Lund, 22100 Lund, Sweden
M. Willatzen
Mads Clausen Institute, University of Southern Denmark, DK-6400 Sønderborg, Denmark
R. Melnik
Wilfrid Laurier University, Waterloo, Ontario N2L 3C5, Canada
L.C. Lew Yan Voon
Department of Physics, Wright State University, Dayton, Ohio 45435

(Received 10 April 2006; accepted 16 August 2006)

An eight-band $k\cdot p$ theory that does not suffer from the spurious solution problem is demonstrated. It is applied to studying the electronic properties of InP and InAs free-standing nanowires. Band gaps and effective masses are reported as a function of size, shape, and orientation of the nanowires. We compare our results with experimental work and with other calculations.

I. INTRODUCTION

In the last few years there has been a resurgence of interest in quantum wires, or nanowires as they are now more commonly called. Those with shorter longitudinal (transverse) aspect ratios are known as quantum rods or nanorods (nanoribbons).

The interest is in part driven by new bottom-up growth methods such as laser-assisted catalytic growth[1,2] and colloidal synthesis,[3,4] and by the demonstration of lasing in ZnO,[5] GaN,[6] and CdS nanowires.[7] The nanowires are now mostly of the free-standing type; typical dimensions are tens of nanometers in lateral linear size and microns in length, although nanowires as small as 3 nm in lateral size have been reported.[1,2] In addition to the cubic semiconductors, nanowires of wirtzite structure have been synthesized. For the most part, they can be assumed to have low defect concentrations and close to bulk crystal structure, although there have been a few reports of strained nanowires.[8] As expected, a number of studies have already been made. Experimentally, examples are polarized photoluminescence[9,10] and Raman scattering.[11]

Surprisingly, the nature of the valence-band states and the calculation of the band gap is still a disputed problem. There were early calculations of the band structures of embedded nanowires using the $k\cdot p$ method. In 1989, Citrin and Chang[12] applied the six-band Luttinger-Kohn $k\cdot p$ to rectangular GaAs/$Al_{0.2}Ga_{0.8}$As nanowires. One result of the latter is that a crossing behavior of the first two valence states in a square quantum wire (because of Γ_6 and Γ_7 symmetries of C_{4v}) becomes anti-crossing in a rectangular quantum wire (because of all states being Γ_5 of C_{2v}). Another result is the mixing of heavy-hole (HH) and light-hole (LH) states even at $k = 0$. Typical cross-sections were 10×10 nm. Sercel and Vahala[13–15] studied cylindrical GaAs/$Al_{0.3}Ga_{0.7}$As nanowires with infinite and finite barriers by using a four-band model within the axial approximation. They went down to 1 nm radius in their calculations, although one might question the applicability of $k\cdot p$ at that point. In k_z-space, their results for the $R = 2.5$- and 5.0-nm nanowires show that the $F_z = 1/2$ state is the lowest in energy at $k_z = 0$, but the $F_z = 3/2$ is lower at finite k_z; this is, in fact, the crossing reported by Citrin and Chang.[12] A number of other articles have now been published in this vein.

More recent calculations for free-standing zinc-blende nanowires are less common. There have been calculations of nanowire band structures using the empirical tight-binding method.[16–18] There are also a few ab initio calculations now reported for InP nanowires,[19,20] though only for the bandgap and not for the whole band structure. The first multiband $k\cdot p$ calculation that we are aware of is one of ours[21] where we introduced the Burt-Foreman Hamiltonian for nanowire calculations. There has also appeared an eight-band $k\cdot p$ calculation[22] that will be discussed later in the article.

In this article we extend our earlier theory by implementing the full eight-band $k\cdot p$ theory. One reason for doing so is that interband optical calculations will incorporate full band-mixing effects.[23] In addition, this is necessary for materials with small gaps; e.g., an InAs/InP nanowire heterostructure has been made recently.[24]

We have three main objectives. One is to report a full eight-band calculation without making the spherical approximation (as was done by Maslov and Ning[22]); this is necessary to get an accurate picture of the orbital nature

[a)]Address all correspondence to this author.
e-mail: benny@mci.sdu.dk
DOI: 10.1557/JMR.2006.0358

of the valence states. We also note that we used the Burt-Foreman Hamiltonian instead of the Luttinger-Kohn Hamiltonian used by Maslov and Ning,[22] and also that the latter studied [001] nanowires, whereas the experimentally grown ones are along [111]. For a study of the differences between results obtained with the Luttinger-Kohn and the Burt-Foreman Hamiltonian for nanowires consult Lassen et al.,[21] and for quantum well structures, see Meney et al.[25] Meney et al.,[25] also compare models using different numbers of bands. Another objective is to compare the band gap of InP nanowires with experimental data[10] and other calculations.[19,20,22] In addition, we report on the electron effective mass dependence on size, as this has not been studied in other articles. Finally, we look briefly into the issue of whether a cylindrical cross-section is an accurate representation of the more appropriate hexagonal one.

II. THEORY

The eight-band $k\cdot p$ theory that we used is based on the exact envelope function theory derived by Burt,[26] the so-called Burt-Foreman Hamiltonian. With respect to the basis $\beta = \{|S\uparrow\rangle, |X\uparrow\rangle, |Y\uparrow\rangle, |Z\uparrow\rangle, |S\downarrow\rangle, |X\downarrow\rangle, |Y\downarrow\rangle, |Z\downarrow\rangle\}$, this theory gives rise to the following Hamiltonian

$$H_8 = \begin{pmatrix} H_4 & 0 \\ 0 & H_4 \end{pmatrix} + H_{\mathrm{SO}} + H_{\mathrm{diag}} \quad , \tag{1}$$

where H_{SO} is the spin-orbit contribution [$H_{\mathrm{SO},ij} = (\hbar^2/4m^2c^2)\langle i \mid (\sigma \times \nabla V)\cdot\vec{k}|j\rangle$] $\vec{k} = i\nabla$, σ is the Pauli spin matrices, V is the crystal potential, m is the free electron mass, c is the speed of light, and $\hbar$ is Planck's constant/2π], H_{diag} is the diagonal matrix with band-edge energies as entries ($H_{\mathrm{diag},ii} = \langle i \mid (\hbar^2/2m)\vec{k}^2 + V \mid i\rangle$), and

In terms of the γ parameters and the Kane energy, E_p, the various parameters are given by

$$L = \frac{\hbar^2}{2m}(\gamma_1 + 4\gamma_2) \quad , \tag{3}$$

$$M = \frac{\hbar^2}{2m}(\gamma_1 - 2\gamma_2) \quad , \tag{4}$$

$$N_1 = -3\frac{\hbar^2}{2m}(\gamma_3 + \chi) \quad , \tag{5}$$

$$N_2 = -3\frac{\hbar^2}{2m}(\gamma_3 + \chi) \quad , \tag{6}$$

$$P = \sqrt{\frac{2m}{\hbar^2}E_p} \quad , \tag{7}$$

where

$$\chi \approx \frac{1}{3}(3\gamma_3 + 2\gamma_2 - \gamma_1 - 1) \quad . \tag{8}$$

Note that the χ parameter appears because we use the exact envelope function approach (see Ref. 27). The γ parameters and A can be found from the Luttinger parameters, γ^L, the Kane energy, E_p, the band gap, E_g, the spin-orbit splitting, Δ_{SO}, and the conduction band effective mass, m_c, according to

$$E_p = \frac{2}{m}\mid\langle S|p_x|X\rangle\mid^2 \quad , \tag{9}$$

$$\gamma_l^L = \gamma_1 + \frac{E_p}{3E_g} \quad , \tag{10}$$

$$H_4 = \begin{pmatrix}
\vec{k}^t\begin{pmatrix}A&0&0\\0&A&0\\0&0&A\end{pmatrix}\vec{k} & i\begin{pmatrix}P\\0\\0\end{pmatrix}^t\vec{k} & i\begin{pmatrix}0\\P\\0\end{pmatrix}^t\vec{k} & i\begin{pmatrix}0\\0\\P\end{pmatrix}\vec{k} \\
-i\vec{k}^t\begin{pmatrix}P\\0\\0\end{pmatrix} & \vec{k}^t\begin{pmatrix}L&0&0\\0&M&0\\0&0&M\end{pmatrix}\vec{k} & \vec{k}^t\begin{pmatrix}0&N_1&0\\N_2&0&0\\0&0&0\end{pmatrix}\vec{k} & \vec{k}^t\begin{pmatrix}0&0&N_1\\0&0&0\\N_2&0&0\end{pmatrix}\vec{k} \\
-i\vec{k}^t\begin{pmatrix}0\\P\\0\end{pmatrix} & \vec{k}^t\begin{pmatrix}0&N_2&0\\N_1&0&0\\0&0&0\end{pmatrix}\vec{k} & \vec{k}^t\begin{pmatrix}M&0&0\\0&L&0\\0&0&M\end{pmatrix}\vec{k} & \vec{k}^t\begin{pmatrix}0&0&0\\0&0&N_1\\0&N_2&0\end{pmatrix}\vec{k} \\
-i\vec{k}^t\begin{pmatrix}0\\0\\P\end{pmatrix} & \vec{k}^t\begin{pmatrix}0&0&N_2\\0&0&0\\N_1&0&0\end{pmatrix}\vec{k} & \vec{k}^t\begin{pmatrix}0&0&0\\0&0&N_2\\0&N_1&0\end{pmatrix}\vec{k} & \vec{k}^t\begin{pmatrix}M&0&0\\0&M&0\\0&0&L\end{pmatrix}\vec{k}
\end{pmatrix} \quad . \tag{2}$$

$$\gamma_2^L = \gamma_2 + \frac{E_p}{6E_g} \quad , \tag{11}$$

$$\gamma_3^L = \gamma_3 + \frac{E_p}{6E_g} \quad , \tag{12}$$

$$\frac{\hbar^2}{2m_c} = A + \frac{\hbar^2}{2m}\left(\frac{2E_p}{3E_g} + \frac{E_p}{3(E_g + \Delta_{SO})}\right) \quad . \tag{13}$$

Nanowires have a periodic crystal structure in the wire direction, and in $k{\cdot}p$ theory, this results in a translational symmetry along the wire. We can use this symmetry to reduce the problem to a two-dimensional problem by writing the eight-band Hamiltonian [Eq. (1)] with respect to coordinates where one axis (e.g., the x_3'-axis) is along the wire direction. We can then separate the envelope function into a part that describes the behavior along the wire and a part that describes the behavior perpendicular to the wire direction, i.e., $F(x_1', x_2', x_3') = e^{ik_{x_3'}x_3'} F(x_1', x_2')$, where x_1', x_2', and x_3' are the new coordinates, $k_{x_3'}$ is a constant, and F is a vector of size 8 consisting of the individual envelope functions. The rotation matrix U that rotates the x_3 axes onto the x_3' axes is given by

$$x_i' = U_{ij}x_j, \quad k_i' = U_{ij}k_j \quad , \tag{14}$$

where

$$U(\phi,\theta) = \begin{pmatrix} \cos(\phi)\cos(\theta) & \sin(\phi)\cos(\theta) & -\sin(\theta) \\ -\sin(\phi) & \cos(\phi) & 0 \\ \cos(\phi)\sin(\theta) & \sin(\phi)\sin(\theta) & \cos(\theta) \end{pmatrix} \quad . \tag{15}$$

The angles θ and ϕ are the conventional angles of rotation shown in Fig. 1. Given a nanowire oriented in a certain direction, we need to determine these angles so that the x_3' axis is parallel to the direction of the nanowire,

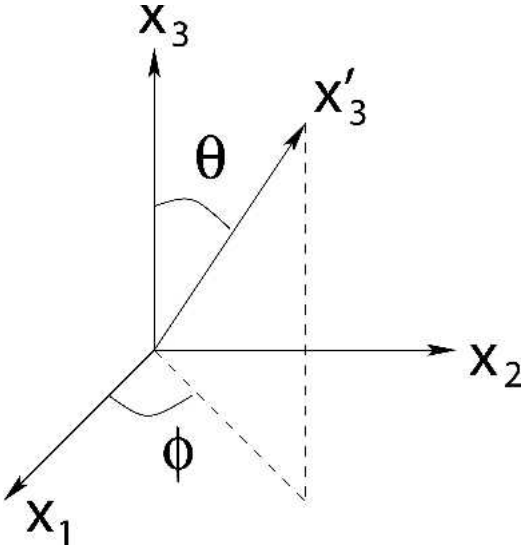

FIG. 1. The angles appearing in the rotation matrix U.

e.g., if the nanowire is oriented in the [110] direction, we find that $\theta = \pi/2$ and $\phi = \pi/4$.

To write everything with respect to the new coordinate system, we introduce the transformation that gives the rotated basis set $\beta' = \{|S'\uparrow'\rangle, |X'\uparrow'\rangle, |Y'\uparrow'\rangle, |Z'\uparrow'\rangle, |S'\downarrow'\rangle, |X'\downarrow'\rangle, |Y'\downarrow'\rangle, |Z'\downarrow'\rangle\}$ in terms of the old basis set β

$$\beta' = W\beta \quad ; \tag{16}$$

$$W = A\hat{U} \quad , \tag{17}$$

where

$$\hat{U}(\phi,\theta) = \begin{pmatrix} 1 & 0_{(1,3)} & 0 & 0_{(1,3)} \\ 0_{(1,3)} & U(\phi,\theta) & 0_{(3,1)} & 0_{(3,3)} \\ 0 & 0_{(1,3)} & 1 & 0_{(1,3)} \\ 0_{(3,1)} & 0_{(3,3)} & 0_{(3,1)} & U(\phi,\theta) \end{pmatrix} \quad , \tag{18}$$

[$0_{(n,m)}$ is the $n \times m$ zero matrix] and

$$A = \begin{pmatrix} e^{-i\frac{\phi}{2}}\cos\left(\frac{\theta}{2}\right)I_4 & e^{i\frac{\phi}{2}}\sin\left(\frac{\theta}{2}\right)I_4 \\ -e^{-i\frac{\phi}{2}}\sin\left(\frac{\theta}{2}\right)I_4 & e^{i\frac{\phi}{2}}\cos\left(\frac{\theta}{2}\right)I_4 \end{pmatrix} \quad . \tag{19}$$

Here I_4 is the 4×4 identity matrix. The transformation W is compsed of the rotation of the $|S\rangle, |X\rangle, |Y\rangle, |Z\rangle$ states (given by $\hat{U}$) and the rotation of the spin (given by A; see Ref. 28).

The transformed eight-band Hamiltonian is then given by

$$\hat{H}_8 = W^*\begin{pmatrix} H_4' & 0_{(4,4)} \\ 0_{(4,4)} & H_4' \end{pmatrix} W^t + H_{SO} + H_{diag} \quad , \tag{20}$$

where H_4' is H_4 written in terms of $\vec{k}' = U^t\vec{k}$, e.g., the element in the first row and first column is given by

$$[H_4']_{11} = \vec{k}'^t U \begin{pmatrix} A & 0 & 0 \\ 0 & A & 0 \\ 0 & 0 & A \end{pmatrix} U^t\vec{k}' \quad , \tag{21}$$

and the other elements are given similarly. In Eq. (20) we have also used that $H_{SO} + H_{diag}$ is invariant with respect to W. Next, we introduce a basis set that diagnolizes the spin-orbit coupling H_{SO}

$$u^c_{1/2,1/2} = |S'\uparrow'\rangle \quad ,$$

$$u^c_{1/2,-1/2} = |S'\downarrow'\rangle \quad ,$$

$$u^v_{3/2,3/2} = \frac{1}{\sqrt{2}}(|X'\uparrow'\rangle + i|Y'\uparrow'\rangle) \quad ,$$

$$u^{\upsilon}_{3/2,1/2} = \frac{1}{\sqrt{6}}\left(|X'\downarrow'\rangle + i|Y'\downarrow'\rangle - 2|Z'\uparrow'\rangle\right) \quad ,$$

$$u^{\upsilon}_{3/2,-1/2} = \frac{1}{\sqrt{6}}\left(-|X'\uparrow'\rangle + i|Y'\uparrow'\rangle - 2|Z'\downarrow'\rangle\right) \quad ,$$

$$u^{\upsilon}_{3/2,-3/2} = \frac{1}{\sqrt{2}}\left(|X'\downarrow'\rangle + i|Y'\downarrow'\rangle\right) \quad ,$$

$$u^{\upsilon}_{1/2,1/2} = \frac{1}{\sqrt{3}}\left(|X'\downarrow'\rangle + i|Y'\downarrow'\rangle + |Z'\uparrow'\rangle\right) \quad ,$$

$$u^{\upsilon}_{1/2,-1/2} = \frac{1}{\sqrt{3}}\left(-|X'\uparrow'\rangle + i|Y'\uparrow'\rangle + |Z'\downarrow'\rangle\right) \quad .$$

The eight-band Hamiltonian finally becomes

$$\tilde{H}_8 = S^* W^* \begin{pmatrix} H'_4 & 0_{(4,4)} \\ 0_{(4,4)} & H'_4 \end{pmatrix} W^t S^t + \begin{pmatrix} E_c I_2 & 0_{(2,4)} & 0_{(2,2)} \\ 0_{(4,2)} & E_\upsilon I_4 & 0_{(4,2)} \\ 0_{(2,2)} & 0_{(2,4)} & (E_\upsilon - \Delta_{SO}) I_2 \end{pmatrix} \quad , \qquad (22)$$

where I_2 and I_4 are the 2×2 and 4×4 identity matrices, respectively, E_c is the conduction band edge, E_υ is the valence-band edge, and

$$S = \begin{pmatrix} 1 & 0 & 0 & 0 & 0 & 0 & 0 & 0 \\ 0 & 0 & 0 & 0 & 1 & 0 & 0 & 0 \\ 0 & \frac{1}{\sqrt{2}} & \frac{1}{\sqrt{2}}i & 0 & 0 & 0 & 0 & 0 \\ 0 & 0 & 0 & -\frac{\sqrt{2}}{\sqrt{3}} & 0 & \frac{1}{\sqrt{6}} & \frac{1}{\sqrt{6}}i & 0 \\ 0 & -\frac{1}{\sqrt{6}} & \frac{1}{\sqrt{6}}i & 0 & 0 & 0 & 0 & -\frac{\sqrt{2}}{\sqrt{3}} \\ 0 & 0 & 0 & 0 & 0 & \frac{1}{\sqrt{2}} & -\frac{1}{\sqrt{2}}i & 0 \\ 0 & 0 & 0 & \frac{1}{\sqrt{3}} & 0 & \frac{1}{\sqrt{3}} & \frac{1}{\sqrt{3}}i & 0 \\ 0 & -\frac{1}{\sqrt{3}} & \frac{1}{\sqrt{3}}i & 0 & 0 & 0 & 0 & \frac{1}{\sqrt{3}} \end{pmatrix} . \qquad (23)$$

III. RESULTS

We have implemented the above eight-band Hamiltonian [Eq. (22)] for free-standing nanowires using a plane-wave expansion inside the first Brillouin zone. We only include plane waves inside the first Brillouin zone as this is demanded by the exact envelope function theory.[26] Also, this ensures that we do not have problems with oscillatory spurious solutions.[29] To model free-standing structures, we chose a large confining potential outside the structure (positive for electron and negative for hole), the free-electron mass as the effective mass for electrons, and minus the free electron mass as effective mass for the holes. Note that the eight coupled equations [the eigenvalue problem using the eight-band Hamiltonian of Eq. (20)] should be written formally in Fourier space and not in real space, as the differential equations suggest that interface boundary conditions are needed and this is incompatible with the requirement that the plan-wave expansion is restricted to the first Brillouin zone. The material parameters are taken from the article by Vurgaftman et al.[30]

In this section, we apply the Hamiltonian equation [Eq. (22)] applicable to (infinite) nanowires grown along an arbitrary direction to determine dispersion curves, effective band gaps, and effective masses at $k = 0$. Results are shown for InP and InAs nanowires grown along the three directions: [111], [110], and [001]. In all cases computed, we assume that electrons and holes are almost completely confined to the nanowire (the barrier potential is set to 6 eV such that the wave functions decay strongly outside of the cylindrical surface). This is consistent with the ab initio results of Schmidt et al.[20] Particular attention is given to the case with circular and hexagonal nanowire cross-sections.

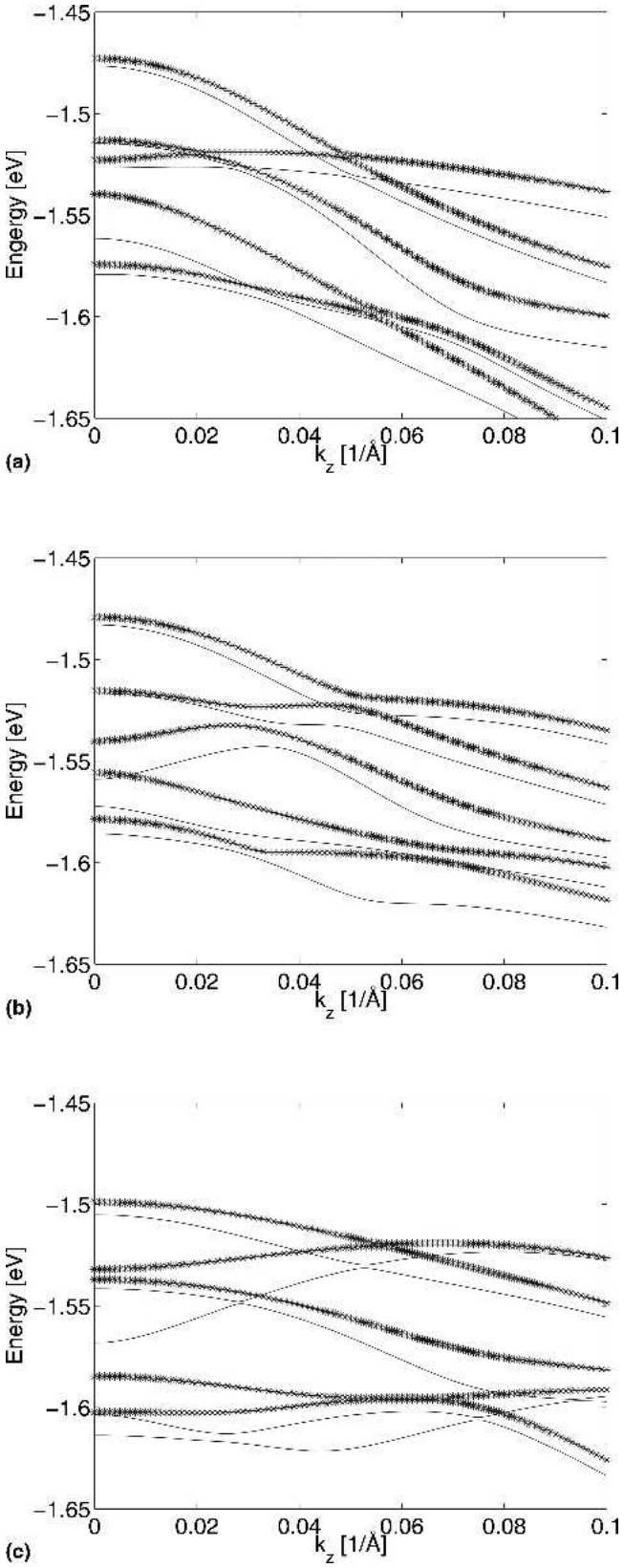

FIG. 2. Band structure of cylindrical InP nanowires of radius 25 Å for three different directions: (a) [111], (b) [110], and (c) [001]. The asterisk and solid line correspond to an 8 × 8 and 6 × 6 matrix calculation, respectively.

In Fig. 2, valence-state dispersion curves for the three directions, [111], [110], and [001], and shown in the (a), (b), and (c) subplots, respectively, corresponding to a InP nanowire with a 50 Å wire diameter. Clearly, band mixing is important, e.g., significant band repulsion takes place at k values close to 0.02 $Å^{-1}$. There is a question as to whether the level crossing reported by Maslov and Ning[22] using a [001] nanowire and the spherical approximation would relat to the correct growth direction ([111]) and theoretical model (no spherical approximation); our calculations show that the crossing is in fact preserved. However, we do find an anti-crossing for [110] growth.

The asterisk and solid lines in Fig. 2 correspond to an 8 × 8 (in the valence p and conduction s states) and a 6 × 6 (in the valence p states) matrix calculation, respectively. Note that the upper part of the valence band structure close to $k = 0$ is almost unaffected by incorporating the conduction-band states among the interesting states. This is reasonable as one would expect limited coupling between conduction s states and valence p band states because InP is a large-bandgap material. The most pronounced influence of the conduction s state is observable for large k values. Note also more pronounced differences between an 8 × 8 band-structure calculation and a 6 × 6 band-structure calculation in the dispersion curves for the more highly excited valence-band states. Finally, the nature of the highest $k = 0$ state is about 90% $|3/2\ 1/2\rangle$-like.

In Fig. 3, we plot the effective band gap of InP nanowire structures, defined as the energy difference between the lowest conduction subband and the topmost valence subband at $k = 0$, as a function of nanowire diameter in the range of 50–500 Å. The curves show the dependencies on the growth directions. Evidently, the energy difference changes rapidly for small nanowire radii (below

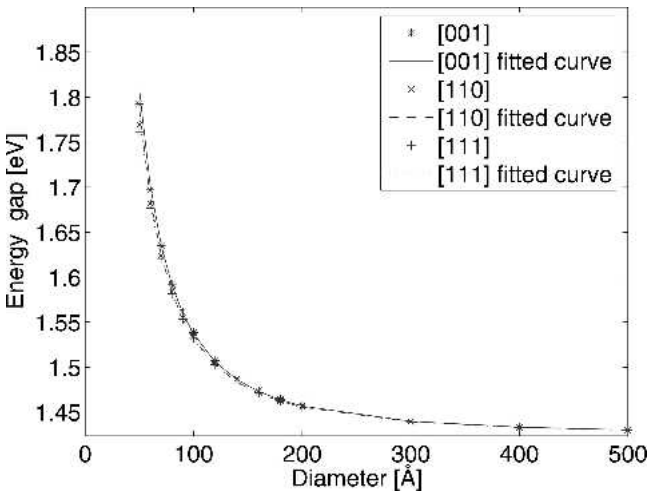

FIG. 3. Diameter dependence of band gap for cylindrical InP nanowires.

approximately 100 Å) while approaching the bulk bandgap of 1.42 eV at large nanowire radii. A similar tendency in effective bandgap dependence on nanowire radius is observed for the three cases of nanowire growth directions.

In Fig. 4, conduction-band effective masses of InP nanowire structures are depicted as a function of the nanowire diameter in the range of 50–500 Å. A one-band calculation with an infinite barrier would give a constant effective mass. It can be observed clearly that the conduction-band states couple, although not strongly, to the valence-band states as expected. Our results show that the effective mass changes from the bulk value of approximately $0.08m_0$ to approximately $0.11m_0$ as the diameter decreases from 500 to 50 Å. The size dependence of the effective mass had previously been reported for quantum wells.[31]

In Table I, we give curve-fit parameters for the effective bandgap and the conduction-band effective mass (obtained from the computed results) for InP nanowires oriented along the three cases of growth directions. The parameters are obtained by fitting to the expressions

$$m_c = a + b \cdot d^{-n}$$

$$E_g^{eff} = a_g + b_g \cdot d^{-n_g}. \quad (24)$$

The bandgaps agree well with the experimental data at $T = 7$K of Gudiksen and coworkers[10] except for an almost constant shift of about 20 meV (experimental gaps being smaller), which can be explained as the excitonic binding energy. Our result for the band-gap variation differs substantially from the one-band result of $n_g = 2$. Note that the two ab initio calculations reported are $n_g = 2$[20] and $n_g = 1.16$–1.36.[19] Thus, more experimental data might be needed to establish the correct scaling.

TABLE I. Curve-fit parameters for the band gap and conduction effective mass of InP nanowires.

	a	b	n	a_g	b_g	n_g
[001]	0.0795	34.7	1.75	1.424	389	1.77
[110]	0.0795	22.8	1.71	1.424	348	1.75
[111]	0.0795	19.3	1.70	1.424	333	1.75

In Fig. 5, valence-band effective masses of InP nanowire structures are shown as a function of the nanowire diameter between 50 and 160 Å. Here, a large anistropy is observed. We see that the valence-band effective masses in the [110] and [111] directions are much lighter than the effective masses in the [001] direction. This is rather surprising, as the highest valence-band state at $k = 0$ is predominantly light-hole like, i.e., $|3/2 \pm 1/2\rangle$-like, in the three directions, and the bulk light hole masses are $0.121m$, $0.055m$, and $0.108m$ for [001], [110], and [111], respectively. This clearly shows that the effective mass of a nanowire is not governed by bulk properties, i.e., whether the wave function is mostly heavy hole-like or light hole-like. Note that the valence-band effective masses are only shown up to a nanowire diameter of 160 Å. The reason for this is that for larger diameters, the distance between sub-bands is so small that valence-band effective masses are not clearly resolved. To illustrate the problem, in Fig. 6, we plot the dispersion curves for a 300 Å InAs nanowire (InAs has been chosen because the problem is most pronounced for this choice of material). For large radii, however, it is again possible to find the effective mass. In Table II, we list the bulk valence-band effective masses together with the effective masses for nanowires with a 500 and 1000 Å diameter. Here, we see that the valence-band effective masses approach the bulk value as the diameter is increased.

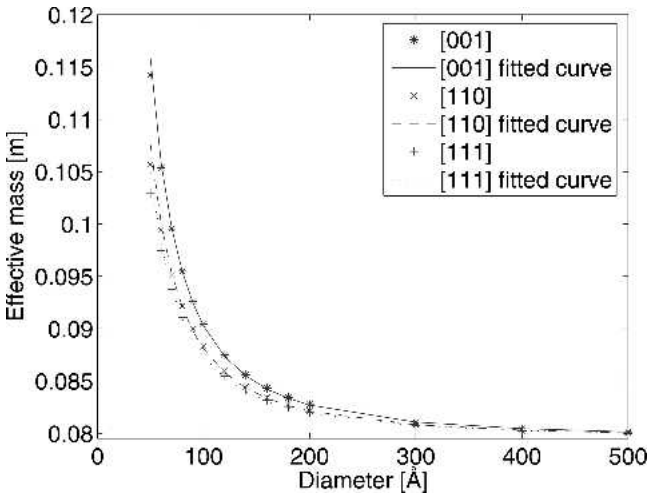

FIG. 4. Diameter dependence of electron effective mass for cylindrical InP nanowires.

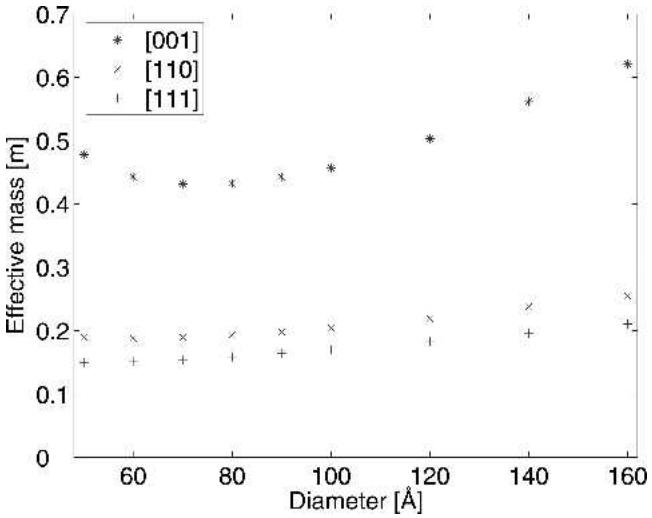

FIG. 5 Diameter dependence of valence-band effective mass for cylindrical InP nanowires.

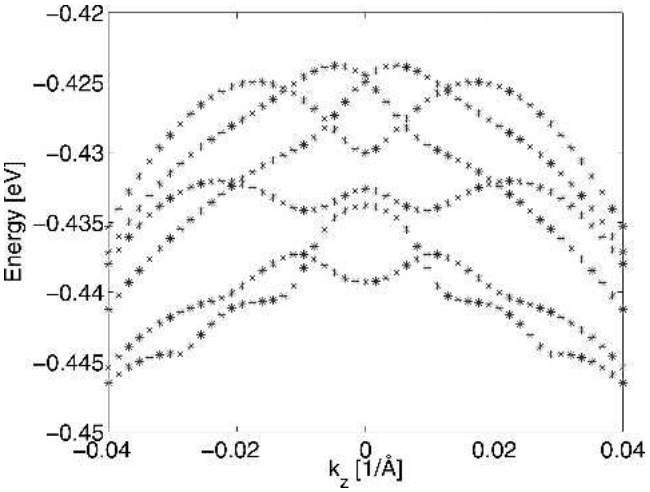

FIG. 6. Dispersion curves for a 300 Å diameter InAs nanowire.

TABLE II. Curve-fit parameters for the band gap and conduction effective mass of InAs nanowires.

	a	b	n	a_g	b_g	n_g
[001]	0.026	28.1	1.54	0.417	164	1.47
[110]	0.026	16.2	1.46	0.417	138	1.44
[111]	0.026	13.7	1.43	0.417	141	1.45

In Fig. 7, a plot of the upper valence-band structure is shown as a function of k value for a [111]-grown InP nanowire structure in cases with a circular (diameter equal to 100 Å) and hexagonal nanowire cross-section. The distance between opposite sides (equal to 97.75 Å) in the hexagonal is fixed such that the lowest subband energy at $k = 0$ coincides with the lowest subband energy of the corresponding circular-shaped nanowire. Evidently, the shape and crossing behavior of the various subbands is more or less independent of the cross-

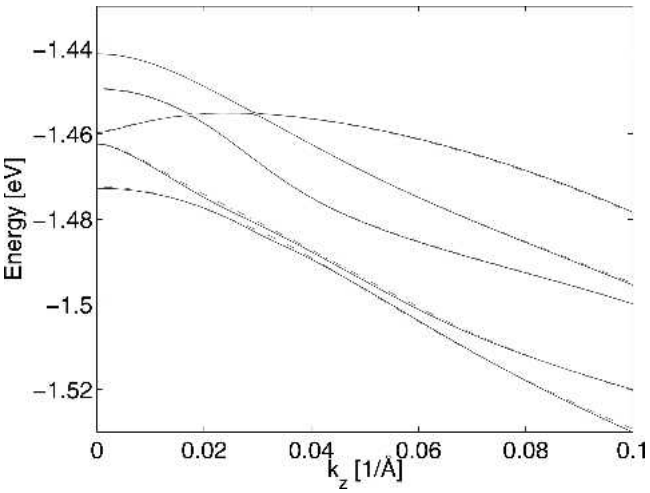

FIG. 7. Comparison of band structure for [111] cylindrical (solid lines) and hexagonal (dashed lines) InP nanowires.

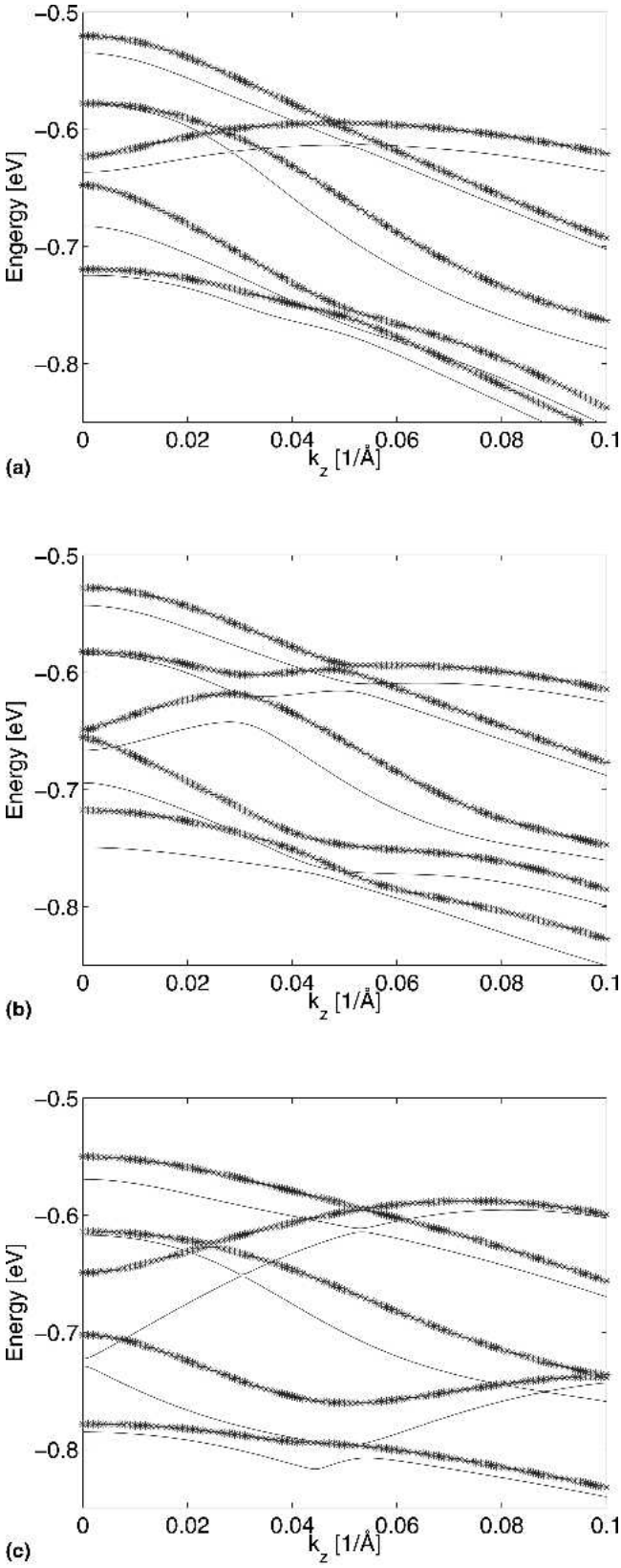

FIG. 8. Band structure of cylindrical InAs nanowires with a radius of 25 Å for three different directions: (a) [111], (b) [110], and (c) [001]. The asterisk and solid line correspond to an 8 × 8 and 6 × 6 matrix calculation, respectively.

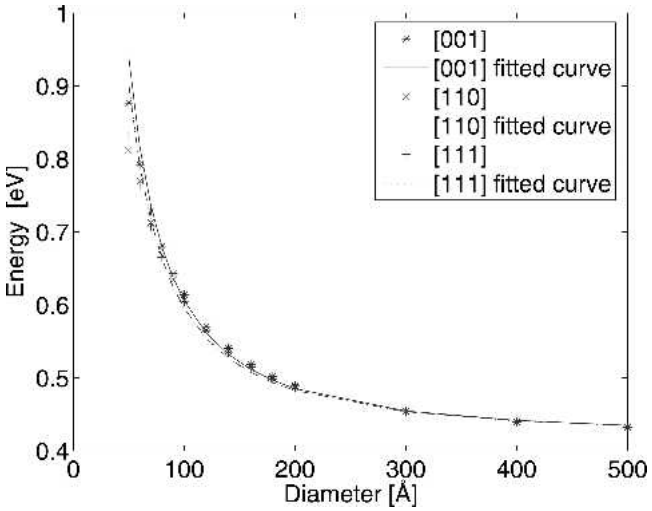

FIG. 9. Diameter dependence of band gap for cylindrical InAs nanowires.

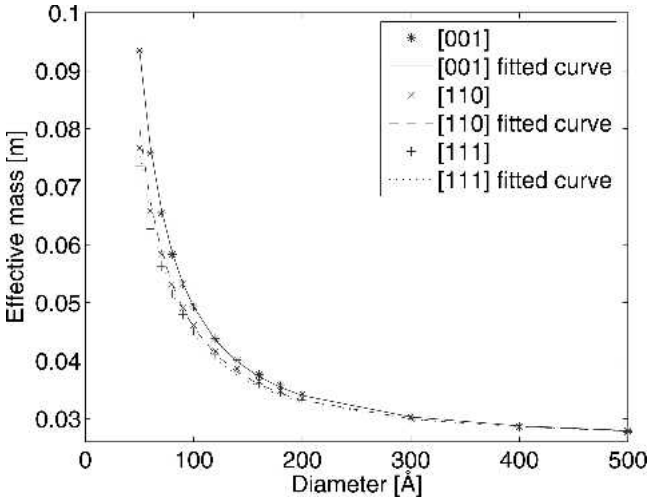

FIG. 10. Diameter dependence of conduction-band effective mass for cylindrical InAs nanowires.

TABLE III. Valence-band effective masses for InP and InAs nanowires with 500 and 1000 Å diameters.

	[001] InP	[110] InP	[111] InP	[001] InAs	[110] InAs	[111] InAs
500 Å	0.6681	1.0153	1.1839	0.4073	0.5876	0.6749
1000 Å	0.5812	0.9513	1.1522	0.3508	0.5333	0.6380
Bulk value	0.5319	0.8850	1.1364	0.3333	0.5128	0.6250

To compare, the bulk values are also given. (The bulk values have been taken from Vurgaftman et al.[30])

sectional shape. We attribute this to the very close symmetry between the hexagonal and circular cross-sections in the (111) plane. In addition, we found that the difference between absolute sub-band energy values is less than 0.02 eV for the k range: 0–0.11 Å^{-1}. Hence, it is appropriate to model [111] nanowires using a circular cross-section.

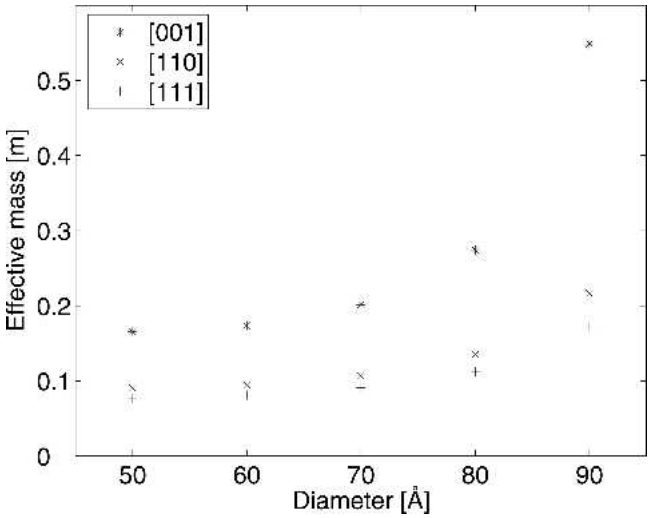

FIG. 11. Diameter dependence of valence-band effective mass for cylindrical InAs nanowires.

To give an example of a material where it is more important to use the 8 × 8 model, we show the results for InAs nanowires. To facilitate a comparison between InAs and InP nanowires, we have included the same figures for InAs as for InP, although we will only briefly comment on the InAs results. In Fig. 8, dispersion curves are shown for InAs nanowires with a diameter of 50 Å oriented in the [111], [110], and [001] directions (a), (b), and (c). Here, we see that there is a much larger discrepancy between the results of 8 × 8 (asterisk lines) and 6 × 6 (solid lines) matrix calculations. Even at $k = 0$, we see a difference of up to 20 meV. The reason for this is that InAs is a narrow band gap material (0.417 eV band gap), and because of this, the conduction band and the valence band cannot be solved separately. In Fig. 9, the band gap, and in Fig. 10, the conduction-band effective masses are shown as functions of the nanowire diameter. As was the case for InP, there is not much difference between the three directions. In Table III, we give the curve-fit parameters, where, again, the band gap and the conduction-band effective masses have been fitted according to the expressions in Eq. (24). In Fig. 11, we show the valence-band effective masses as a function of the nanowire diameter. Here, we see that for small nanowires, there is no large difference between the effective masses in the three directions. However, as the diameter is increased, the effective mass in the [001] direction grows at a much faster rate than the effective mass in the [110] and the [111] directions, resulting in an increased anisotropy.

IV. CONCLUSIONS

Dispersion curves, effective bandgaps, and effective masses are computed for free-standing InP and InAs nanowire structures as a function of orientation, shape, and size based on an 8 × 8 Hamiltonian description

where spurious-state problems are circumvented (by inclusion of first Brillouin-zone plane-wave contributions to the envelope functions only). Our Hamiltonian and method for eliminating spurious solutions are more fundamentally sound than those of Maslov and Ning.[22] There are differences in the bandgaps and effective masses when comparing results for [001], [110], and [111] directions. A comparison between an 8×8 and an 6×6 Hamiltonian analyses shows that discrepancies in the valence band are most pronounced for nanowires grown along the [001] direction. Even though InP is a large bandgap material, we found that the conduction mass can be significantly enhanced over the bulk value for small nanowires, and for InAs, this was even more pronounced. For InAs, we also found that there were significant differences between 8×8 and 6×6 models, even at $k = 0$. Hence, we conclude that an eight-band model is essential, particularly for small nanostructures. Finally, our calculated size dependence of the bandgap of [111] nanowires is consistent with the experimental data of Gudiksen and coworkers,[10] but not with other calculations.

ACKNOWLEDGMENTS

The work was supported by National Science Foundation CAREER award (Grant No. 0454849) and by a Research Challenge grant from Wright State University and the Ohio Board of Regents.

REFERENCES

1. A.M. Morales and C.M. Lieber: A laser ablation method for the synthesis of crystalline semiconductor nanowires. *Science* **279**(5348), 208 (1998).
2. X. Duan and C.M. Lieber: General synthesis of compound semiconductor nanowires. *Adv. Mater.* **12**(4), 298 (2000).
3. J. Hu, L-S. Li, W. Yang, L. Manna, L-W. Wang, and A.P. Alivisatos: Linearly polarized emission from colloidal semiconductor quantum rods. *Science* **292,** 2060 (2001).
4. D. Katz, T. Wizansky, O. Millo, E. Rothenberg, T. Mokari, and U. Banin: Size-dependent tunneling and optical spectroscopy of CdSe quantum rods. *Phys. Rev. Lett.* **89**(8), 086801-1 (2002).
5. M.H. Huang, S. Mao, H. Feick, H. Yan, Y. Wu, H. Kind, E. Weber, R. Russo, and P. Yang: Room-temperature ultraviolet nanowire nanolasers. *Science* **292**(5523), 1897 (2001).
6. J.C. Johnson, H-J. Choi, K.P. Knutsen, R.D. Schaller, P. Yang, and R.J. Saykally: Single gallium nitride nanowire lasers. *Nat. Mater.* **1**(2), 106 (2002).
7. X. Duan, Y. Huang, R. Agarwal, and C.M. Lieber: Single-nanowire electrically driven lasers. *Nature* **421,** 241 (2003).
8. H.W. Seo, S.Y. Bae, J. Park, H. Yang, K.S. Park, and S. Kim: Strained gallium nitride nanowires. *J. Chem. Phys.* **116**(21), 9492 (2002).
9. Y. Wang, L. Zhang, C. Liang, G. Wang, and X. Peng: Catalytic growth and photoluminescence properties of semiconductor single-crystal ZnS nanowires. *Chem. Phys. Lett.* **317**(3–4), 314 (2002).
10. M.S. Gudiksen, J. Wang, and C.M. Lieber: Size-dependent photoluminescence from single indium phosphide nanowires. *J. Phys. Chem. B* **106**(16), 4036 (2002).
11. R. Gupta, Q. Xiong, C.K. Adu, U.J. Kim, and P.C. Eklund: Laser-induced fano resonance scattering in silicon nanowires. *Nano Lett.* **3**(5), 627 (2003).
12. D.S. Citrin and Y-C. Chang: Valence-subband structures of GaAs/$Al_xGa_{1-x}As$ quantum wires: The effect of split-off bands. *Phys. Rev. B* **40**(8), 5507 (1989).
13. P.C. Sercel and K.J. Vahala: Analytical technique for determining the polarization dependence of optical matrix elements in quantum wires with band-coupling effects. *Appl. Phys. Lett.* **57**(6), 545 (1990).
14. P.C. Sercel and K.J. Vahala: Analytical technique for determining quantum-wire and quantum-dot band structure in the multiband envelope-function representation. *Phys. Rev. B* **42**(6), 3690 (1990).
15. P.C. Sercel and K.J. Vahala: Polarization dependence of optical absorption and emission in quantum wires. *Phys. Rev. B* **44**(11), 5681 (1991).
16. M.P. Persson and H.Q. Xu: Electronic structure of nanometer-scale GaAs whiskers. *Appl. Phys. Lett.* **81**(7), 1309 (2002).
17. M.P. Persson and H.Q. Xu: Giant polarization anisotropy in optical transitions of free-standing inp nanowires. *Phys. Rev. B* **70,** 161310(R) (2004).
18. M.P. Persson and H.Q. Xu: Electronic structure of [100]-oriented free-standing semiconductor nanowires. *Nano Lett.* **4**(12), 2409 (2004).
19. J. Li and L-W. Wang: Band-structure-corrected local density approximation study of semiconductor quantum dots and wires. *Phys. Rev. B* **72**(12), 125325 (2005).
20. T.M. Schmidt, R.H. Miwa, P. Venezuela, and A. Fazzio: Stability and electronic confinement of free-standing inp nanowires: *Ab initio* calculations. *Phys. Rev. B* **72**(16), 193404 (2005).
21. B. Lassen, L.C. Lew Yan Voon, R. Melnik, and M. Willatzen: Exact envelope-function theory versus symmetrized Hamiltonian for quantum wires: A comparison. *Solid State Commun.* **132,** 141 (2004).
22. A.V. Maslov and C.Z. Ning: Radius-dependent polarization anisotropy in semiconductor nanowires. *Phys. Rev. B* **72**(16), 161310(R) (2005).
23. L.C. Lew Yan Voon, M. Willatzen, M. Cardona, and L.R. Ram-Mohan: Comment on "multiband coupling effects on electron quantum well intersubband transitions." *J. Appl. Phys.* **80**(1), 600 (1996).
24. M.T. Björk, B.J. Ohlsson, T. Sass, A.I. Persson, C. Thelander, M.H. Magnusson, K. Deppert, L.R. Wallenberg, and L. Samuelson: One-dimensional steeplechase for electrons realized. *Nano Lett.* **2,** 87 (2002).
25. A.T. Meney, B. Gonul, and E.P. O'Reilly: Evaluations of various approximations used in the envelope-function method. *Phys. Rev. B* **50,** 10893 (1994).
26. M.G. Burt: The justification for applying the effective-mass approximation to microstuctures. *J. Phys.: Condens. Matter* **4,** 6651 (1992).
27. E.P. Pokatilov, V.A. Fonoberov, V.M. Fomin, and J.T. Devreese: Development of an eight-band theory for quantum dot heterostructures. *Phys. Rev. B* **64,** 245328 (2001).
28. E.O. Kane: Energy band structure in *p*-type germanium and silicon. *J. Phys. Chem. Solid.* **1,** 82 (1956).
29. W. Yang and K. Chang: Origin and elimination of spurious solutions of the eight-band $k \cdot p$ theory. *Phys. Rev. B* **72**(3), 233309 (2005).
30. I. Vurgaftman, J.R. Meyer, and L.R. Ram-Mohan: Band parameters for III–V compound semiconductors and their alloys. *J. Appl. Phys.* **89,** 5815 (2001).
31. G. Hendorfer, M. Seto, H. Ruckser, W. Jantsch, M. Helm, G. Brunthaler, W. Jost, H. Obloh, K. Kohler, and D.J. As: Enhancement of the in-plane effective mass of electrons in modulation-doped In_xGa_{1-x} as quantum wells due to confinement effects. *Phys. Rev. B* **48**(4), 2328 (1993).